Journal of Alloys and Compounds 509 (2011) 1430–1435

Contents lists available at ScienceDirect

Journal of Alloys and Compounds

journal homepage: www.elsevier.com/locate/jallcom

Spectroscopic studies of $KGd(WO_4)_2:Ho^{3+}$ single crystals

D. Kasprowicz[a], M.G. Brik[b,*], A. Majchrowski[c], E. Michalski[c], A. Biadasz[a]

[a] Faculty of Technical Physics, Poznan University of Technology, Nieszawska 13 A, 60 - 965 Poznań, Poland
[b] Institute of Physics, University of Tartu, Riia 142, Tartu 51014, Estonia
[c] Institute of Applied Physics, Military University of Technology, Kaliskiego 2, 00 - 908 Warszawa, Poland

ARTICLE INFO

Article history:
Received 21 September 2010
Received in revised form 3 November 2010
Accepted 5 November 2010
Available online 13 November 2010

Keywords:
Absorption and luminescence spectra
Rare-earth doped crystals
Judd–Ofelt theory

ABSTRACT

Single crystals of $KGd(WO_4)_2$ doped with Ho^{3+} ions were grown by the top seeded solution growth method. Polarized room temperature absorption spectra were analyzed by means of the conventional Judd–Ofelt theory taking into account strong dependence of the host refractive index on the wavelength. In addition to the intensity parameters Ω_2, Ω_4, Ω_6, the branching ratios and radiative lifetimes were estimated for all possible transitions in the studied spectral region. The transitions predicted by the phenomenological model as potential transitions for laser applications are discussed. Emission spectra in the green, red, and near-infrared spectral regions were recorded for different excitation wavelengths. Comparison with spectroscopic properties of Ho^{3+} ion in other crystals is discussed.

1. Introduction

Potassium gadolinium tungstate crystals $KGd(WO_4)_2$ (KGW) doped with different rare earth ions attract considerable interest due to their potential for the solid state laser materials [1]. It was found that doping KGW with trivalent lanthanides leads to a high efficiency of stimulated emission at low pumping energies with laser diode excitation [2]. KGW is an optically biaxial crystal. Some linear optical properties of KGW crystals are reported in Ref. [3]; in particular, the orientation of the optical indicatrix of the crystal with respect to the crystallographic axes was determined [3]. Dependence of the refractive indices in the visible and near-infrared regions was measured and the refractive index variations were modeled by an infrared-corrected Sellmeier equation [3]. Several papers devoted to the studies of the structure, optical and spectroscopic properties of pure and lanthanide doped KGW were published recently [3–12]. In this work we present the analysis of the $KGW:Ho^{3+}$ room temperature absorption spectra using the conventional Judd–Ofelt theory and actual dependence of the refractive index on the wavelength. In this way, we estimated the Judd–Ofelt intensity parameters, branching ratios and radiative lifetimes for all transitions in the studied spectral range. The emission cross-sections for the optical transitions in the visible region were estimated from the analysis of the luminescence spectra.

* Corresponding author.
E-mail addresses: dobroslawa.kasprowicz@put.poznan.pl (D. Kasprowicz), brik@fitartu.ee (M.G. Brik).

0925-8388/$ – see front matter
doi:10.1016/j.jallcom.2010.11.053

2. Crystal growth and crystal structure

$KGW:Ho^{3+}$ single crystal were obtained by means of the top seeded solution growth (TSSG) method from 25 mol% solutions of KGW in $K_2W_2O_7$ on the [0 1 0] oriented seeds under low temperature gradients conditions. Owing to mild temperature gradients the KGW single crystals were confined with crystallographic faces. The pulled up crystals grew on the (0 1 0) plane that formed flat interface. This allowed avoiding non-uniform distribution of dopants, as it is often encountered when the interface is formed by several crystallographic faces characterized with different distribution coefficients. The detailed description of this technique can be found elsewhere [13]. The doping concentration of Ho^{3+} ions was 1 at.%, which amounted to 0.08 mol/l. The size of the crystal cut for the spectroscopic measurements was 4.28 mm × 4.40 mm × 4.09 mm (along the *a* and *b* crystallographic axes, and *c** axis perpendicular to the *ab* plane).

KGW crystal at room temperature has a monoclinic structure with the $C2/c \equiv C_{2h}^6$ space group. The crystal lattice constants are: $a = 10.652$ Å, $b = 10.374$ Å, $c = 7.582$ Å, $\beta = 130.80°$ [14]. In the host crystal structure the tungsten and oxygen atoms form octahedral anionic complexes with C_1 symmetry. The potassium K^+ and gadolinium Gd^{3+} ions occupy randomly the equivalent crystallographic positions with the C_2 symmetry. The structure of KGW is formed by chains of $W_2O_8{}^{4-}$ ions along the *c*-axis and connected in their corners by WOW oxygen bridge bonds. The $W_2O_8{}^{4-}$ dimers are formed by two $WO_4{}^{2-}$ ions, which are connected by the "WOOW" double oxygen bridge bonds. Along the *b* axis the tungstate–oxygen layers are alternated with the cationic layers created by K^+ and Gd^{3+} ions. From the point of view of electrical charge, ionic radii and nature of the substituting and substituted ions it is natural that the Gd^{3+} ions can be substituted by Ho^{3+} ions [3,5]. Fig. 1 depicts a unit cell of KGW crystal with coordination polyhedra around Gd^{3+} ions.

3. Experimental spectroscopic results

The room-temperature absorption spectra of KGW:Ho^{3+} crystal were recorded using a Cary 400 spectrophotometer in the 300–800 nm spectral range. Absorption spectra were recorded for three possible orientation of the sample: the incident light was parallel to the a, b axes and c^* direction of the crystal. Fig. 2 shows the absorption spectra of KGW:Ho^{3+}. As seen from these figures, the spectra are quite anisotropic, from the point of view of intensities of the absorption bands. Ho^{3+} absorption in the spectral region below 300 nm is hidden due to the host's strong absorption (mainly caused by the tetragonal $(WO_4)^{2-}$ groups).

The most intensive absorption transition is at about 450 nm and is assigned to the transition from the $^5I_8$ ground state of Ho^{3+} ion to the $^5G_6$ and $^5F_1$ manifolds. Two well-separated absorption peaks at about 650 nm and 550 nm are due to the transitions to the $^5F_5$ and $^5F_4$, $^5S_2$ manifolds. A group of very weak lines at about 460–480 nm was attributed to transitions to three manifolds $^3K_8$, $^5F_3$, $^5F_2$. A peak at about 420 nm is assigned to the $^5G_5$ level, although it should be emphasized that the wave function of this state is an almost 1:1 mixture of two states: $^5G_5$ and $^3G_5$. Calculations of the free Ho^{3+} ion energy levels performed by means of diagonalization of a standard Hamiltonian give the following composition of a wave function for this level (only three leading contributions are shown): $-0.63475|^5G_5\rangle - 0.44578|^3G(2)_5\rangle - 0.38609|^5F_5\rangle + \ldots$. On the other hand, the $|^5G_5\rangle$ state also produces the main contribution to another state at about 28,000 cm^{-1}, whose wave function is $-0.70070|^5G_5\rangle + 0.39736|^3H(4)_5\rangle + 0.30291|^3G(2)_5\rangle + \ldots$. These examples emphasize that the mixture of different states plays an important role and should be thoroughly taken into account, especially when describing the high-lying energy levels of trivalent lanthanides. Finally, moving further to higher energies, one finds a weak line at about 385 nm (transitions to the $^3K_7$, $^5G_4$ manifolds) and a more intensive line at about 360 nm ($^3H_6$, $^5G_5$ levels).

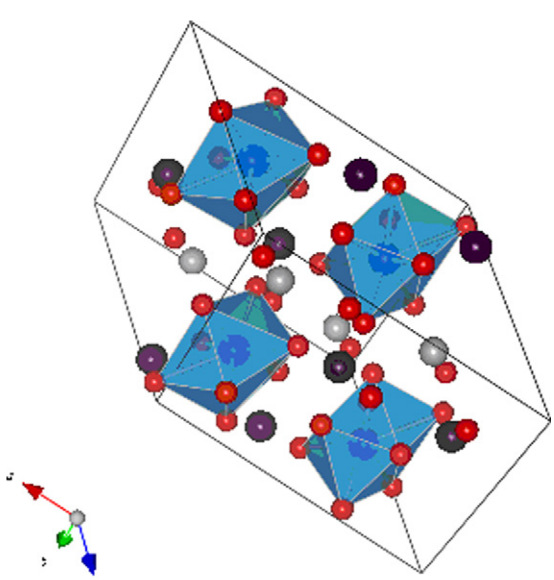

Fig. 1. One unit cell of $KGd(WO_4)_2$ crystal. Tungstate ions are in black, potassium ions in grey, gadolinium ions are at the centers of the oxygen polyhedra.

4. Judd–Ofelt analysis

Detailed analysis of the absorption spectra recorded at room temperature was performed using the conventional Judd–Ofelt theory [15,16] and actual dependence of the refractive index on the wavelength [3]. The oscillator strength f_{calc} of an electric-dipole transition between two states $|4f^N(\alpha' S' L')J'\rangle$ and $|4f^N(\alpha SL)J\rangle$ of an ion with N f-electrons is given by the following equation:

$$f_{calc} = \frac{8\pi^2 mc\nu}{3h(2J'+1)}\chi \sum_{\lambda=2,4,6} \Omega_\lambda |\langle 4f^N(\alpha SL)J||U^{(\lambda)}||4f^N(\alpha' S' L')J'\rangle|^2, \quad (1)$$

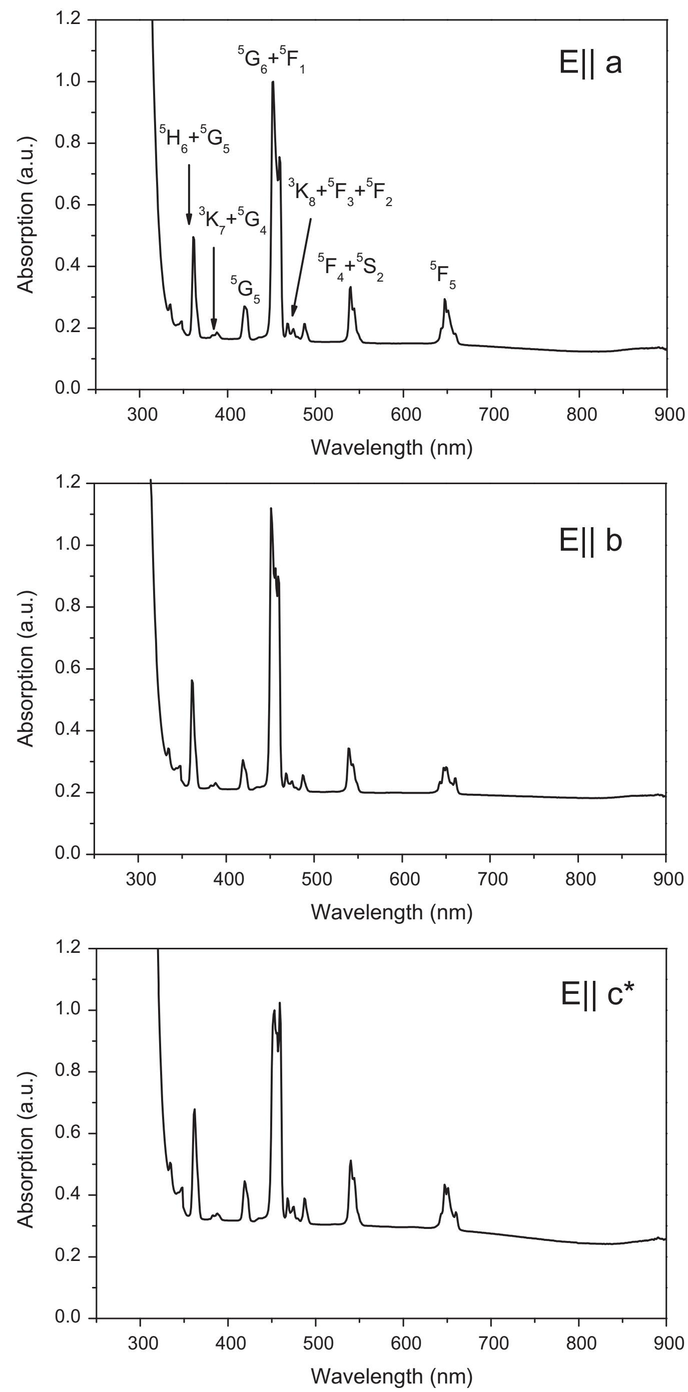

Fig. 2. The room-temperature absorption spectra of KGW:Ho^{3+}. The polarization of each spectrum is shown in the figure. Absorption peaks assignment in the two lowest figures is the same as in the upper figure.

Table 1
Squares of reduced matrix elements of the unit tensor operators U^2, U^4, and U^6 for Ho^{3+} (the first, second and third rows for each manifold, respectively). Refer to the text for explanation regarding the $^5G_5$ states.

J manifold	$^5I_8$	$^5I_7$	$^5I_6$	$^5I_5$	$^5I_4$	$^5F_5$	$^5F_4$	$^5S_2$	$^3K_8$	$^5F_3$	$^5F_2$	$^5G_6$	$^5F_1$	$^5G_5$	$^3K_7$	$^5G_4$	$^3H_6$	$^5G_5$
	0.193998	0.024852	0.008399	0	0	0	0	0	0.021194	0	0	1.473151	0	0	0.005800	0	0.261609	0
$^5I_8$	0.310255	0.134173	0.038500	0.008756	0.000001	0.418169	0.239455	0	0.032720	0	0	0.815722	0	0.528145	0.004485	0.035758	0.144196	0.091512
	1.537831	1.519985	0.691261	0.098422	0.007945	0.561487	0.708272	0.206874	0.159816	0.346367	0.211480	0.143498	0	0.000071	0.034147	0.033490	0.001735	0.162246
		0.149879	0.031701	0.003030	0	0.019440	0	0	0.002035	0	0	0.146766	0	0.573470	0.005745	0	0.033183	0.693874
$^5I_7$		0.119088	0.133184	0.024658	0.003341	0.327941	0.196717	0	0.004567	0.247813	0	0.424394	0	0.023939	0.006146	0.288505	0.061915	0.191066
		0.029573	0.930799	0.877508	0.157030	0.442562	0.032398	0.428435	0.040557	0.227985	0.075137	0.262404	0.057325	0.116269	0.005103	0.064422	0.007614	0.057074
			0.126894	0.042961	0.002350	0.011596	0.001151	0	0.005978	0	0	0.009216	0	0.129659	0.001194	0.694734	0.000169	0.093838
$^5I_6$			0.067493	0.166709	0.028490	0.127178	0.257581	0.026171	0.004071	0.089801	0.136655	0.082237	0	0.169623	0.005646	0.023268	0.005707	0.243018
			0.040863	0.584967	0.665048	0.483828	0.170781	0.140122	0.012839	0.217431	0.166405	0.108317	0.240674	0.081645	0.071460	0.000533	0.003025	0.045211
				0.103551	0.030943	0.006029	0.001267	0	0	0.000006	0	0.014169	0	0.003897	0.007187	0.223636	0.000577	0.004482
$^5I_5$				0.038012	0.123807	0.028979	0.131001	0.005537	0.000408	0.220082	0.046650	0.028958	0.140064	0.065100	0.003959	0.271071	0.001095	0.051025
				0.020509	0.912675	0.161764	0.463453	0.089674	0.003478	0.018336	0.316393	0.012043	0.167361	0.060717	0.029380	0.031133	0.013816	0.041406
					0.122248	0.000082	0.000171	0.001434	0	0.000217	0.000476	0.000499	0	0	0	0.015332	0.000038	0.003527
$^5I_4$					0.131357	0.005608	0.023736	0.033188	0.004702	0.097767	0.198901	0.001317	0.144401	0.009008	0.000593	0.107689	0.000028	0.009824
					0.344718	0.005008	0.258421	0.287080	0.001213	0.397191	0.026510	0.000064	0	0.042251	0.006190	0.055633	0.020651	0.000788
						0.072538	0.199354	0	0	0.039852	0	1.126711	0	0.342730	0.001676	0.036976	0.114810	0.088359
$^5F_5$						0.177263	0.094099	0.012863	0.026531	0.077815	0.005263	0.367319	0.00010	0.033695	0.011609	0.015443	0.000036	0.173084
						0.003589	0.008555	0.006726	0.020756	0.084338	0.141681	0.031603	0.118257	0.113870	0.015195	0.218226	0.000245	0.045660
							0.077411	0.000048	0	0.097717	0.008746	0.251123	0	0.275176	0	0.397900	0.011259	0.296474
$^5F_4$							0.008652	0.017395	0.008010	0.029916	0.079053	0.235502	0.047233	0.023598	0.015876	0.105046	0.022593	0.002467
							0.089805	0.003880	0.000630	0.095801	0.031582	0.128718	0	0.139768	0.008989	0.021875	0.026645	0.051458
								0.000080	0	0.007270	0.001678	0	0.011881	0	0	0.036193	0	0
$^5S_2$								0.001926	0	0.000079	0.003819	0.308873	0	0.101372	0	0.283139	0.045277	0.053939
								0	0.000539	0	0	0.005787	0	0.000477	0.055411	0.023983	0.007452	0.000718
									0.027890	0	0	0.000003	0	0	0.087677	0	0.111955	0
$^3K_8$									0.048687	0	0	0.005081	0	0.009075	0.000366	0.090717	0.108795	0.005516
									0.216511	0.005850	0.003315	0.319409	0	0.001019	0.134731	0.001525	1.574961	0.021828
										0.036387	0.051817	0	0.008446	0.179450	0	0.216917	0	0.154178
$^5F_3$										0.064121	0.000010	0.064952	0.059199	0.101921	0.006732	0.018338	0.011541	0.046129
										0.027211	0	0.152943	0	0.033285	0.004920	0.050609	0.052040	0.005658
											0.007576	0	0.053119	0	0	0.258125	0	0
$^5F_2$											0.027089	0.025038	0	0.149278	0	0.000613	0.006929	0.123871
											0	0.100802	0	0.010722	0.050320	0.118709	0.010712	0.001530
												0.002963	0	0.055750	0.000037	0.003670	0.052241	0.000522
$^5G_6$												0.382221	0	0.260015	0.000383	0.205814	0.307599	0.067156
												0.121129	0.052618	0.244661	0.128280	0.292754	0.007514	0.157094
													0.030342	0	0	0	0	0
$^5F_1$													0	0.007155	0	0.056590	0	0.007381
													0	0.052996	0.001774	0	0.000108	0.056012
														0.074252	0.016734	0.012294	0.201171	0.025648
$^5G_5$														0.049125	0.005660	0.149941	0.064009	0.013155
														0.015765	0.250656	0.025161	0.020813	0.202116
															0.001933	0	0.003090	0.003749
$^3K_7$															0.024359	0.015426	0.049891	0.010289
															0.021206	0.003996	0.690862	0.494649
																0.009465	0.002942	0.040957
$^5G_4$																0.013992	0.005741	0.143520
																0.179816	0.008989	0.017398
																	0.144569	0.149342
$^3H_6$																	0.094678	0.584843
																	0.037612	0.000007
																		0.037311
$^5G_5$																		0.004952
																		0.001158

Table 2
Calculated and measured oscillator strengths and the values of refractive index for the absorption bands for the KGW:Ho^{3+}. The root mean square deviation between the calculated and experimental oscillator strengths is 1.39×10^{-6}.

Absorption band (from the $^5I_8$ ground state to the final level)	Refractive index	Barycenter (cm^{-1})	f_{exp} (10^{-6})	f_{calc} (10^{-6})
$^5F_5$	2.046	15,360	5.0836	4.9111
$^5F_4 + ^5S_2$	2.068	18,509	5.8276	6.4095
$^3K_8 + ^5F_3 + ^5F_2$	2.089	20,942	4.8275	5.0287
$^5G_6 + ^5F_1$	2.100	21,987	53.5590	54.1670
$^5G_5$	2.120	23,807	5.03550	5.4818
$^3K_7 + ^5G_4$	2.149	25,951	1.5935	1.1923
$^3H_6 + ^5G_5$	2.174	27,611	17.6900	15.1248

where m is the electron's mass, c stands for the speed of light, h is the Planck's constant, ν is the barycenter of the absorption band (in cm^{-1}), J' is the value of the total angular momentum of the ground manifold and $\chi = ((n^2+2)^2)/9n$ is the local field correction factor. The reduced matrix elements of the unit tensor operators $U^{(\lambda)}$ were recalculated in the intermediate coupling approximation (which takes into account strong mixture of different states with the same values of J shown in the previous section) using the free ion's Hamiltonian parameters from Ref. [17]; their numerical values for the J manifolds in the considered spectra region are given in Table 1. Experimental oscillator strengths f_{exp} were extracted from the absorption spectra using the following expression:

$$f_{exp} = \frac{4.319 \times 10^{-9}}{Cd} \int \varepsilon(\sigma) d\sigma, \tag{2}$$

where $\varepsilon(\sigma)$ is the molar absorptivity at energy σ (this energy is expressed in cm^{-1}); C is the rare earth ion concentration (mol/l); d is the optical path length (in cm). Since the absorption spectra are different for different orientations of the samples (Fig. 2), the values of f_{exp} were averaged over three polarizations and were then used for the Judd–Ofelt analysis. The calculated and experimentally deduced oscillator strengths are shown in Table 2. Actual dependence of the refractive index on the wavelength from Ref. [3] was taken into account.

Table 3 collects the values of the Judd–Ofelt intensity parameters (in cm^2) for Ho^{3+} in KGW obtained in the present work in comparison with other available literature data for this and other compounds.

As seen from Table 3, the Ω_4 and Ω_6 parameters are close to each other in all hosts (apart from the last shown host KPb_2Cl_5), though the values of Ω_2 are more different. According to Refs. [24,25], the Ω_2 parameter is sensitive to the local structure around a rare earth ion. Such a variety of the Ω_2 values suggest various degrees of deformation around Ho^{3+} ion in all these materials, which can be readily explained by different electric charges and ionic radii of Ho^{3+} and substituting ions. Increasing values of the Ω_2 parameter are also related to increase of the asymmetry of the rare earth ion site and increase of covalency [26,27]. At the same time, the two remaining parameters Ω_4 and Ω_6 depend on the bulk properties of the host and are affected by vibrations of the nearest neighbors [28]. In this way it becomes clear why these parameters are more or less close for all hosts in which oxygen ions are the nearest neighbors of Ho^{3+}. Only when the ligands are changed to Cl (the last column of the table), a more noticeable change in Ω_4 and Ω_6 values occurs.

After the Judd–Ofelt intensity parameters $\Omega_\lambda (\lambda = 2, 4, 6)$ are determined, it becomes easy to calculate the radiative lifetimes of the excited J manifolds. The radiative transition probability from the state $\langle f^N[\gamma, S, L]J|$ to the state $|f^N[\gamma', S', L']J'\rangle$ can be calculated as follows:

$$A_{JJ'} = \frac{64\pi^4 e^2 \nu^3}{3h(2J+1)} \frac{n(n^2+2)^2}{9} \times \sum_{\lambda=2,4,6} \Omega_\lambda \langle f^N[\gamma, S, L]J||U^\lambda||f^N[\gamma', S', L']J'\rangle^2, \tag{3}$$

where e is the charge of electron, and all other quantities are the same as in Eq. (1). Summing up the $A_{JJ'}$ quantities over all possible final states, one can get the radiative lifetime τ of an excited energy level as

$$\tau = \frac{1}{\sum_{J'} A_{JJ'}} \tag{4}$$

Finally, the branching ratio $\beta_{JJ'}$ defined as

$$\beta_{JJ'} = \frac{A_{JJ'}}{\sum_{J'} A_{JJ'}} \tag{5}$$

shows a contribution of a particular radiative transition from the excited manifold J to all terminal states of the J' manifold.

The results of the τ, $A_{JJ'}$ and $B_{JJ'}$ calculations for KGW:Ho^{3+} are collected in Table 4. If – for a particular transition – the branching ratio is about or greater than 0.5 (or 50%), such a transition can be considered as a potential lasing transition [29,30]. Such a condition is met for several transitions in the KGW:Ho^{3+} host, for example, for the $^3G_5 \rightarrow ^5I_7$ (at about 18,750 cm^{-1}), $^5G_6 + ^5F_1 \rightarrow ^5I_8$ (at about 21,987 cm^{-1}), $^3K_8 + ^5F_3 + ^5F_2 \rightarrow ^5I_8$ (at about 20,942 cm^{-1}), $^5F_4 + ^5S_2 \rightarrow ^5I_8$ (at about 18,500 cm^{-1}), $^5F_5 \rightarrow ^5I_8$ (at about 15,360 cm^{-1}), $^5I_6 \rightarrow ^5I_8$ (at about 8580 cm^{-1}) transitions.

5. Emission spectra

Room temperature emission spectra of KGW:Ho^{3+} were recorded with HITACHI F-4500 Fluorescence Spectrophotometer equipped with xenon lamp and Hamamatsu R928F photomultiplier as a detector. The measurements were carried out for different excitations from 200 to 900 nm spectral range and are shown in Fig. 3. Four different excitation wavelengths have been used: 452, 459, 468, and 488 nm. Assignment of the most prominent emission

Table 3
Comparison of the Judd–Ofelt intensity parameters (in 10^{-20} cm^2) for Ho^{3+} in several materials.

Parameter	KGW, this work	KGW [18]	$Y_3Al_5O_{12}$ [19]	SANZ[a] [20]	Bi_2TeO_5[b] [21]	$SrWO_4$ [22]	KPb_2Cl_5 [23]
Ω_2	10.14	15.35	0.101	5.84	0.715	11.24	1.30
Ω_4	3.09	3.79	2.086	2.38	2.16	3.95	1.34
Ω_6	1.99	1.69	1.724	1.75	1.81	1.23	1.06

[a] SANZ stands for the $45SiO_2$–$10Al_2O_3$–$15Na_2O$–$30ZnF_2$–$0.5Ho_2O_3$ glass.
[b] Averaged over three polarizations.

Table 4
Branching ratios and radiative lifetimes estimations for Ho^{3+} in KGW.

Initial state	Final state[a]	ν (cm^{-1})	A (s^{-1})	β
$^3H_6+^5G_5$, $\tau = 8\ \mu s$	$^5I_8$	27,611	48,942	0.399
	$^5I_7$	22,554	60,004	0.489
	$^5I_6$	19,031	7509.1	0.061
	$^5I_5$	16,453	818.00	0.007
	$^5I_4$	14,391	173.83	0.001
	$^5F_5$	12,251	2561.5	0.021
	$^5F_4+^5S_2$	9102	1479.3	0.012
	$^3K_8+^5F_3+^5F_2$	6669	985.10	0.008
	$^5G_6+^5F_1$	5624	182.80	0.001
	$^3G_5+^5G_5$	3804	75.700	0.0006
	$^3K_7+^5G_4$	1660	7.1000	0.0
			$\sum_{J'} A_{JJ'} = 1.227\times10^5$	
$^3K_7+^5G_4$, $\tau = 20\ \mu s$	$^5I_8$	25,951	3843.8	0.078
	$^5I_7$	20,894	7396.0	0.150
	$^5I_6$	17,371	27,148	0.549
	$^5I_5$	14,793	7327.9	0.148
	$^5I_4$	12,731	854.70	0.017
	$^5F_5$	10,591	721.90	0.015
	$^5F_4+^5S_2$	7442	1569.5	0.032
	$^3K_8+^5F_3+^5F_2$	5009	509.10	0.010
	$^5G_6+^5F_1$	3964	63.200	0.001
	$^3G_5+^5G_5$	2144	6.3000	0.0
			$\sum_{J'} A_{JJ'} = 49,440$	
$^5G_5$, $\tau = 22\ \mu s$	$^5I_8$	23,807	14,412.6	0.323
	$^5I_7$	18,750	24,131.0	0.541
	$^5I_6$	15,227	4041.3	0.091
	$^5I_5$	12,649	407.9	0.009
	$^5I_4$	10,587	72.8	0.002
	$^5F_5$	8447	1239.4	0.028
	$^5F_4+^5S_2$	5298	272.2	0.006
	$^3K_8+^5F_3+^5F_2$	2865	32.7	0.001
	$^5G_6+^5F_1$	1820	5.9	0.0
			$\sum_{J'} A_{JJ'} = 44,616$	
$^5G_6+^5F_1$, $\tau = 9\ \mu s$	$^5I_8$	21,987	1.0070e+05	0.857
	$^5I_7$	16,930	9143.7	0.078
	$^5I_6$	13,407	3020.7	0.026
	$^5I_5$	10,829	2110.5	0.018
	$^5I_4$	8767	599.80	0.005
	$^5F_5$	6627	1795.3	0.015
	$^5F_4+^5S_2$	3478	104.70	0.001
	$^3K_8+^5F_3+^5F_2$	1045	1.9000	0.0
			$\sum_{J'} A_{JJ'} = 1.175\times10^5$	
$^3K_8+^5F_3+^5F_2$, $\tau = 41\ \mu s$	$^5I_8$	20,942	13,760	0.560
	$^5I_7$	15,885	5358.2	0.218
	$^5I_6$	12,362	2981.1	0.121
	$^5I_5$	9784	1446.7	0.059
	$^5I_4$	7722	795.0	0.032
	$^5F_5$	5582	185.8	0.008
	$^5F_4+^5S_2$	2433	22.4	0.001
			$\sum_{J'} A_{JJ'} = 24,550$	
$^5F_4+^5S_2$, $\tau = 53\ \mu s$	$^5I_8$	18,509	13,352	0.707
	$^5I_7$	13,452	3688.0	0.195
	$^5I_6$	9929	1171.8	0.062
	$^5I_5$	7351	440.80	0.023
	$^5I_4$	5289	175.10	0.009
	$^5F_5$	3149	47.900	0.003
			$\sum_{J'} A_{JJ'} = 18,876$	
$^5F_5$, $\tau = 153\ \mu s$	$^5I_8$	15,360	5001.5	0.767
	$^5I_7$	10,303	1251.3	0.192
	$^5I_6$	6780	245.6	0.038
	$^5I_5$	4202	18.4	0.003
	$^5I_4$	2140	0.1	0.0
			$\sum_{J'} A_{JJ'} = 6517$	
$^5I_4$, $\tau = 4$ ms	$^5I_8$	13,220	25.0	0.101
	$^5I_7$	8163	115.7	0.468
	$^5I_6$	4640	92.4	0.374
	$^5I_5$	2062	13.4	0.054
			$\sum_{J'} A_{JJ'} = 247$	
$^5I_5$, $\tau = 2$ ms	$^5I_8$	11,158	170.5	0.413
	$^5I_7$	6101	224.1	0.543
	$^5I_6$	2578	18.5	0.045
			$\sum_{J'} A_{JJ'} = 413$	
$^5I_6$, $\tau = 2$ ms	$^5I_8$	8580	456.6	0.902
	$^5I_7$	3523	49.8	0.098
			$\sum_{J'} A_{JJ'} = 506.4$	

Table 4 (*Continued*)

[a] The $^5I_7$, $^5I_6$, $^5I_5$, $^5I_4$ manifolds are beyond the spectral region studied in the present paper and their positions were evaluated using the free-ion Hamiltonian parameters from Ref. [17].

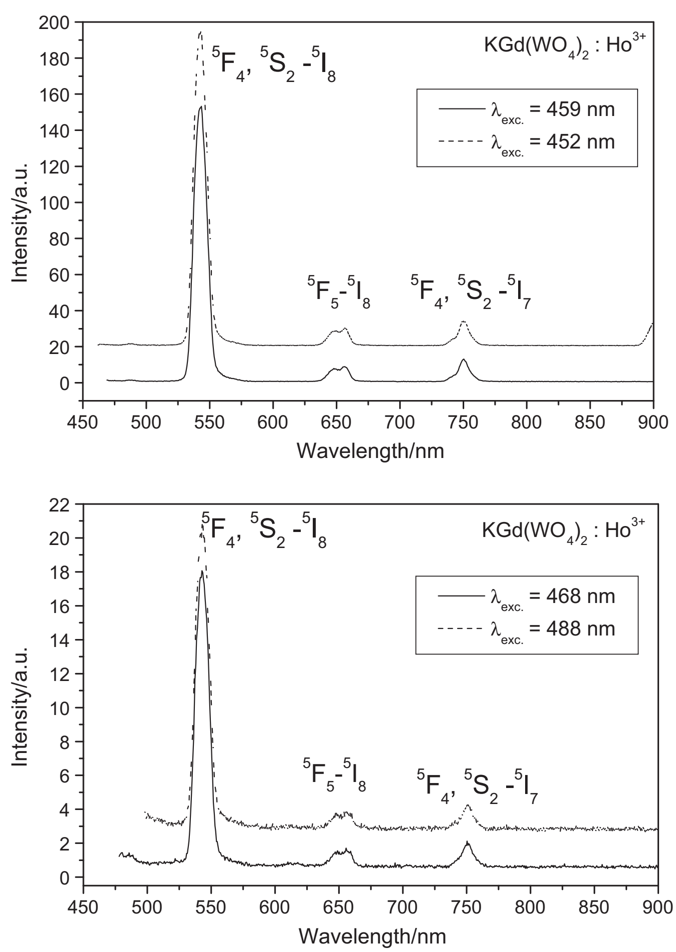

Fig. 3. Room-temperature emission spectra of KGW:Ho^{3+} for different excitation wavelengths. Note the difference in the emission intensity among the four shown spectra.

peaks is straightforward and coincides with previously reported in the literature. A very intensive green emission peak at about 540 nm is due to the $^5F_4$, $^5S_2 \rightarrow {}^5I_8$ transition. The two upper levels $^5F_4$ and $^5S_2$ are located very closely, and both of them contribute to this emission transition at room temperature. However, at low temperature the population of the upper $^5F_4$ level decreases and contribution from the $^5S_2$ manifold determines the overall intensity and emission of the green peak around 540 nm. A weaker red emission band at about 650 nm is assigned to the $^5F_5 \rightarrow {}^5I_8$ transition, and, finally, a near-infrared band at about 750 nm is caused by the $^5F_4$, $^5S_2 \rightarrow {}^5I_7$ transition (again, at high temperature it is practically impossible to distinguish between the contributions from both excited states).

It is easy to see that excitation at 452 and 459 nm results in much higher luminescence intensity (almost one order of magnitude difference), than excitation at longer wavelengths 468 and 488 nm.

One of the characteristics of the emission transitions is the emission cross-section σ_p, evaluated as [31]

$$\sigma_p = \frac{\lambda_p^4}{8\pi c n^2 \Delta\lambda_{eff}} A_{rad} \tag{6}$$

where λ_p is the emission peak's wavelength, $\Delta\lambda_{\mathrm{eff}}$ is the effective line width of the emission band, A_{rad} stands for the probability of the corresponding radiative transition, c and n are the speed of light and index of refraction, respectively. Eq. (6) allows to estimate σ_p for the $^5F_4$, $^5S_2 \rightarrow {}^5I_8$ transition as 3.0×10^{-20} cm^2, which can be compared with the values from 0.95×10^{-20} cm^2 to 2.64×10^{-20} cm^2, estimated for the same transition of Ho^{3+} ion in Ref. [32] in different alkali, mixed alkali and calcium phosphate glasses. The estimated value of σ_p for the $^5F_5 \rightarrow {}^5I_8$ transition is 1.4×10^{-20} cm^2, which also falls within the range from 0.89×10^{-20} cm^2 to 3.06×10^{-20} cm^2 from Ref. [32] for the same transition. Finally, estimations of σ_p for the $^5F_4$, $^5S_2 \rightarrow {}^5I_7$ transition yield the value of about 3.7×10^{-20} cm^2.

Large values of the estimated cross-sections (together with high values of the branching ratios) show that the $^5F_4$, $^5S_2 \rightarrow {}^5I_8$, $^5F_4$, $^5S_2 \rightarrow {}^5I_7$, and $^5F_5 \rightarrow {}^5I_8$ transitions can be used as lasing transitions.

Greater (in comparison with glasses) values of σ_p for KGW:Ho^{3+} show that Ho luminescence in an ordered host is more efficient than in amorphous materials. The possible reasons can be an influence of the ordered arrangement of the crystal lattice ions on the Ho^{3+} energy level structure and well-controlled growth process, which results in a considerably less random distribution of impurity ions in a host.

6. Conclusion

Crystal growth and detailed experimental spectroscopic studies performed using the Judd–Ofelt theory for the $KGd(WO_4)_2$ single crystals doped with Ho^{3+} ions are reported in the present paper. Absorption spectra of the studied crystals recorded at room temperature in the IR, visible and near UV spectral regions exhibit anisotropic properties. The experimental oscillator strengths extracted from three spectra in different polarizations were averaged and used for the Judd–Ofelt calculations. The intensity parameters $\Omega_\lambda(\lambda = 2, 4, 6)$ were compared with available literature data. Calculations of the radiative transition probabilities, excited state lifetimes and branching ratios for all excited states in the considered spectral region from 300 to 800 nm were performed; emission cross-sections for the most intensive peaks in the luminescence spectra were estimated.

Acknowledgement

This work was supported by the Research Project of the Polish Ministry of Sciences and Higher Education: N N202 105336.

References

[1] A.A. Kaminskii, L. Li, A.V. Butashin, V.S. Mironov, A.A. Pavlyuk, S.N. Bagayev, K. Ueda, Opt. Rev. 4 (1997) 309.
[2] C. Pujol, M. Aguiló, F. Díaz, C. Zaldo, Opt. Mater. 13 (1999) 33.
[3] M.C. Pujol, M. Rico, C. Zaldo, R. Solé, V. Nikolov, X. Solans, M. Aquiló, F. Díaz, Appl. Phys. B 68 (1999) 187.
[4] M. Rico, M.C. Pujol, X. Mateos, J. Massons, C. Zaldo, M. Aguiló, F. Díaz, J. Alloys Compd. 323–324 (2001) 362.
[5] L. Macalik, J. Hanuza, A.A. Kaminskii, J. Raman Spectrosc. 33 (2002) 92.
[6] X. Mateos, M.C. Pujol, F. Güell, R. Solé, J. Gavalda, J. Massons, M. Aguiló, F. Díaz, Opt. Mater. 27 (2004) 475.
[7] F. Güell, X. Mateos, Jna. Gavaldà, R. Solé, M. Aguiló, F. Díaz, J. Massons, J. Lumin. 106 (2004) 109.
[8] F. Güell, X. Mateos, Jna. Gavaldà, R. Solé, M. Aguiló, F. Díaz, M. Galan, J. Massons, Opt. Mater. 25 (2004) 71.
[9] J. Lancok, C. Garapon, V. Vorliček, M. Jelinek, M. Čerňanskỳ, Opt. Mater. 28 (2006) 360.
[10] D. Kasprowicz, S. Mielcarek, A. Majchrowski, E. Michalski, M. Drozdowski, Cryst. Res. Technol. 41 (2006) 541.
[11] L. Macalik, P.E. Tomaszewski, R. Lisiecki, J. Hanuza, J. Solid State Chem. 181 (2008) 2591.
[12] A.A. Kaminski, J.B. Gruber, S.N. Bagaev, K. Ueda, U. Hömmerich, J.T. Seo, T. Temple, B. Zandi, A.A. Kornienko, E.B. Dunina, A.A. Pavlyuk, R.F. Klevtsova, F.A. Kuznetsov, Phys. Rev. B 65 (2002) 125108.
[13] A. Majchrowski, M.T. Borowiec, E. Michalski, J. Cryst. Growth 264 (2004) 201.
[14] E. Michalski, A. Majchrowski, J. Appl. Cryst. 36 (2003) 255.
[15] B.R. Judd, Phys. Rev. 127 (1962) 750.
[16] G.S. Ofelt, J. Chem. Phys. 37 (1962) 511.
[17] W.T. Carnall, G.L. Goodman, K. Rajnak, R.S. Rana, J. Chem. Phys. 90 (1989) 3443.
[18] M.C. Pujol, J. Massons, M. Aguilo, F. Diaz, M. Rico, C. Zaldo, IEEE J. Quant. Electron. 38 (2002) 93.
[19] B.M. Walsh, G.W. Grew, N.P. Barnes, J. Phys. Chem. Solids 67 (2006) 1567.
[20] L. Feng, J. Wang, Q. Tang, L. Liang, H. Liang, Q. Su, J. Lumin. 124 (2007) 187.
[21] I. Földvari, A. Baraldi, R. Capelletti, N. Magnani, R.F. Sosa, A.F. Munoz, L.A. Kappers, A. Watterich, Opt. Mater. 29 (2007) 688.
[22] J. Li, G. Jia, Z. Zhu, Z. You, Y. Wang, B. Wu, C. Tu, J. Phys. D: Appl. Phys. 40 (2007) 1902.
[23] D.K. Sardar, S.R. Chandrasekharan, K.L. Nash, J.B. Gruber, A. Burger, U.N. Roy, J. Appl. Phys. 103 (2008) 093112.
[24] W.F. Krupke, Phys. Rev. 145 (1966) 325.
[25] R.C. Powell, Physics of Solid-State Laser Materials, Springer-Verlag, 1998.
[26] S. Tanabe, T. Ohyagi, N. Soga, T. Hanada, Phys. Rev. B 46 (1992) 3305.
[27] H. Ebendorff-Heidepriem, D. Ehrt, M. Bettinelli, A. Speghini, J. Non-Cryst. Solids 240 (1998) 66.
[28] G.V. Prakash, Mater. Lett. 46 (2000) 15.
[29] J.L. Adam, W.A. Sibley, J. Non-Cryst. Solids 76 (1985) 267.
[30] V.R. Kumar, N. Veeraiah, B.A. Rao, S. Buddhudu, J. Mater. Sci. 33 (1998) 2659.
[31] R.D. Peacock, in: J.D. Dunitz, et al. (Eds.), Structure and Bonding, vol. 22, Springer, Berlin, 1975, p. 83.
[32] M. Seshadri, Y.C. Ratnakaram, D. Thirupathi Naidu, K. Venkata Rao, Opt. Mater. 32 (2010) 535.